Modeling Nanoelectromechanical Switches With Random Surface Roughness

Daniel Connelly and Tsu-Jae King Liu, *Fellow, IEEE*

***Abstract*— Surface roughness is an important physical feature of nanometer-scale electromechanical (NEM) devices but typically is not considered in their numerical analysis. In this paper, computer simulations of a single-pole double-throw NEM switch with surface roughness are presented. Roughness is shown to modify the eigenfrequencies of the system, and also to make it possible for the switch to not close successfully. The importance of avoiding a free-standing cantilever is demonstrated.**

***Index Terms*— Logic devices, nanoelectromechanical (NEM) devices, simulation.**

I. Introduction

THE advantages of nanoelectromechanical (NEM) switches over transistors, which make them attractive for ultralow-power digital logic applications, include zero OFF-state leakage and supersteep (nearly zero) subthreshold swing, with stable operation over a wide range of temperatures [1], and reduced device count per digital logic function [2]. The recent introduction of air-gapped interconnects into a CMOS back-end-of-line (BEOL) technology [3] paves a technological pathway for the monolithic integration of NEM switches with CMOS circuitry [4], which can provide for dramatic improvements in energy efficiency [5].

Surface roughness is an important physical feature of nanometer-scale structures, but typically has not been considered in modeling studies due to the difficulty of specifying realistic, randomly unsmooth surfaces. In this paper, the effect of surface roughness on a single-pole double-throw NEM switch is investigated using COMSOL [6]. A method of creating the surface distortion is described, and device modeling results are presented. The importance of torsional compliance in the structure becomes evident only when surface roughness is included.

II. NEM Structure

The NEM switch studied herein is assumed to be formed from three copper metal layers and two copper metal plug ("via") layers using an advanced BEOL technology. The lower two metal layers are used for electrostatic actuation, while the uppermost metal layer is used for signal transmission (i.e., conducting current). A dielectric (SiO_2) post is used to connect the portion of the movable structure formed in the uppermost metal layer to the portion of the movable structure formed in the middle metal layer, to electrically insulate the conducting portion from the actuation portion.

A rendering of the NEM switch structure is shown in Fig. 1. The x-component of the deformation associated with surface roughness modeling is shaded. The substrate is modeled as overlapping broad cones, providing relatively rigid structural support; the cone sidewalls are modeled with antireflective boundaries to promote the dissipation of acoustic waves, and the cone bottom faces are mechanically anchored. The vias formed in the lower via layer are narrower than those formed in the upper via layer, for greater structural compliance. Surface roughness is independently implemented along the x- and y-axes (normal to the z "depth" axis).

III. Surface Roughness Modeling

A. Motivation

In modeling, it is common to make simplifying assumptions about the structure. Real structures are lumpy, with nominal dimensions that represent optimistic targets. It is generally hoped that simulation of the nominal design will correspond to the centroid of the statistical distribution of devices, but the accuracy of this assumption is dubious. For example, consider the case where a response y is a linear function of the dimension x. There are two components, one with $x_1 = x_0 - \Delta x$ and the other with $x_2 = x_0 + \Delta x$. A summed response proportional to $x_1 + x_2$ will be proportional to $2x_0$, independent of Δx which cancels. However, if a response is proportional to the sum of the reciprocals of the dimension $1/x_1 + 1/x_2$, then

$$\begin{aligned} y &\propto \frac{1}{x_0 + \Delta x} + \frac{1}{x_0 - \Delta x} \\ &= \frac{2x_0}{x_0^2 - \Delta x^2} \\ &= \frac{2/x_0}{1 - (\Delta x/x_0)^2} \\ &\approx 2/x_0[1 + (\Delta x/x_0)^2]. \end{aligned} \tag{1}$$

The fraction $\Delta x/x_0$ directly increases the response by a second-order term; therefore, the nominal device represents the lower bound on the response instead of the mean response.

Manuscript received November 26, 2016; revised January 13, 2017 and February 22, 2017; accepted February 23, 2017. Date of current version April 19, 2017. This work was supported by NSF under Grant CHE-0840505. The review of this paper was arranged by Editor F. Ayazi.

The authors are with the Department of Electrical Engineering and Computer Sciences, University of California at Berkeley, Berkeley, CA 94720, USA.

Color versions of one or more of the figures in this paper are available online at http://ieeexplore.ieee.org.

Digital Object Identifier 10.1109/TED.2017.2682644

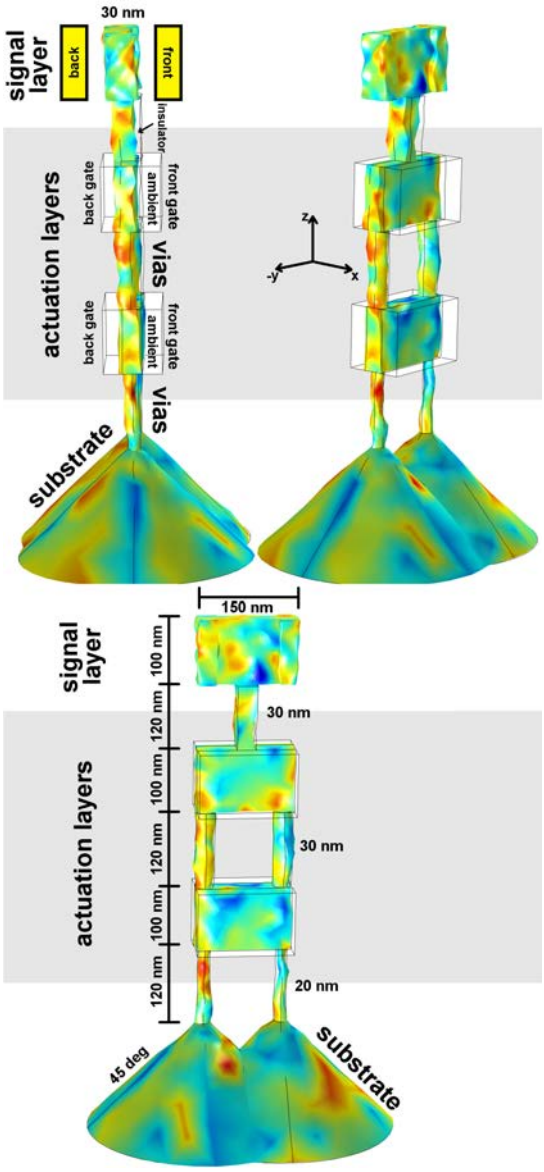

Fig. 1. Simulated NEM switch structure actuated along the x-axis direction. The color (shading) represents the x-component of surface roughness. The actuation (gate) electrodes located on either side (in front/back) of the movable (cantilever) structure, as well as the front and back pairs of contacting electrodes, are modeled analytically and are thus represented schematically here. Only the cantilever structure is physically modeled.

Likewise, a realistic representation of surface roughness may be necessary to characterize a typical NEM device.

An additional effect of surface roughness is to break physical symmetry. For example, consider a structure that is laterally symmetric but torsionally compliant: torsional vibration modes would never be excited due to the structural symmetry; however, torsional modes would be prone to excitation with surface roughness, which is more realistic. The effect of a small asymmetry could be emulated by slightly reducing the contact gap locally at one side of the structure, for example with the addition of a hemispherical surface feature. However, modeling surface roughness in a more realistic random fashion is desirable to more accurately capture real nonideal behaviors.

It should be noted that in [7], surface roughness is considered in detail for modeling of contact resistance, which is dominated by asperities on the contacting surfaces. The methods in that prior work apply to the phenomenon of charge transfer, while this paper focuses on mechanical effects.

B. Modeling Approach

Since BEOL layers are planarized, surface roughness along the z-axis is assumed to be negligible. Roughness is modeled herein only along the x- and y-axes, each as a function of position in all three directions.

As an alternative to specifying a pattern of surface roughness, one could directly emulate the effect of geometric surface perturbations using a noise-based model, for example, the impedance field method [8]. However, this approach would fail to capture second-order effects of the perturbation. As can be seen from the simplified example of (1), the second-order effects are important when perturbations in physical dimensions are significant.

Therefore, surface roughness can be explicitly modeled in two ways: either as a 2-D function applied parametrically over a surface, or as a 3-D function applied to all points in a volume. The latter approach is simpler and is the one used herein. In this way, when the surface is deformed so are the underlying spatial points: a point immediately below the surface will move with the surface, points further below the surface will move in a correlated way with the surface, and points sufficiently far from the surface will move in manner uncorrelated with the surface.

This brings up an important characteristic of surface roughness: although it is random, it is spatially correlated. If you know the displacement of a point $\boldsymbol{r}$, the displacement of a point $\boldsymbol{r} + \Delta\boldsymbol{r}$ will approach the same value as $|\Delta\boldsymbol{r}|$ becomes sufficiently smaller than λ, where λ is a scalar correlation length.

Using COMSOL, spatial distortion can be modeled in one of two ways. The first is to shift the material: on an atomic basis, individual atoms are moved. The second is to shift only the boundaries of the material, filling or removing material to accommodate local volume changes. The former approach introduces local strain fields, while the latter does not. The latter approach is the one which is taken herein, as roughness does not necessarily imply strain.

To model surface roughness, 2-D functions are used, one for perturbations along the x-axis and the other for perturbations along the y-axis, with characteristic parameters of a root-mean-squared amplitude and a correlation length (or separate correlation lengths for the three directions). Following this approach, a sheet with thickness much smaller than the correlation length would have strongly correlated opposite surfaces. The correlation length is assumed to be constant along a particular axis, no matter whether that correlation is tangential to a nominal surface (for example, in the $\hat{y}$-direction on a surface normal to the x-axis) or through a material (for example, opposite surfaces of a thin sheet) or across an air gap. (In reality, these three types of surface correlations may differ.) Additionally, the surface roughness is assumed to be

independent of the material and layer, to preserve functional continuity. For simplicity, to be able to handle surfaces of arbitrary shape and orientation, the displacement is considered to be a single 3-D function for each of the two modeled axes, independent of material.

Two methods for generating a correlated analytic function are as follows.

1) Generate spatially uncorrelated displacements over a discrete mesh, then apply a numerical smoothing function, for example a convolution with a truncated 3-D Gaussian function, for spatial correlation.
2) Work in the Fourier domain by determining spatial boundaries for the unit cell, then randomly determine $\boldsymbol{k}$-space amplitudes with a truncated Gaussian envelope designed to attenuate components of high spatial frequency. The resulting Fourier function is an analytic real-space function with the desired correlation lengths.

The second approach is used herein, since it has the advantage that the function is fully independent of the mesh, as long as the mesh is adequately dense (spacing $\ll \lambda$). Also, applying a Gaussian convolution to an unstructured 3-D mesh is complicated.

The Fourier function used is the following, where δ_i is the component of a displacement $\boldsymbol{\delta}$ along the axis i (here i is either the x- or y-axis):

$$\delta_i = \sum_{n=1}^{N} a_{in} \sin(k_{xn}x + k_{yn}y + k_{zn}z + \phi_{in}). \qquad (2)$$

This is a sum over a set of N points in 3-D $\boldsymbol{k}$-space. That set could comprise a full-factorial sampling of $\boldsymbol{k}$-space for the values of $\boldsymbol{k}$ of sufficiently small magnitude to make a significant contribution, or the sum could be over a subsampling of these values. A full sampling of 3-D $\boldsymbol{k}$-space is computationally burdensome: for example, if each axis were sampled with 40 points, 64 000 points would need to be evaluated involving up to three sine values (for roughness along each of three axes), for a total of 192 000 sines for each mesh point. For the purpose of achieving a "realistic" surface roughness function, this is unnecessary. A realistic function can be attained with a substantial decimation of this 3-D $\boldsymbol{k}$-space; for example, herein 8192 points were selected at random from the ellipsoid in $\boldsymbol{k}$-space where (for scalar λ) $|\lambda \boldsymbol{k}|$ is less than 3, with $\boldsymbol{k}$ values discretized to increments of $2\pi\ \mu\text{m}^{-1}$ along each axis.

The phase terms ϕ and the amplitudes a also were randomly determined. The phases were each chosen with uniform probability from 0 to 2π. The amplitudes were chosen using a unit normal random value multiplied by an envelope function $\exp[-(k_x^2\lambda_x^2 + k_y^2\lambda_y^2 + k_z^2\lambda_z^2)/2]$. This causes the high spatial frequency components of the Fourier function to rapidly attenuate, leading to spatial correlation. The use of a Gaussian autocorrelation function has a long history [9], but is a simplification [10].

A hazard with this Fourier-domain function generation approach is that the function can lead to structural singularities, which cause the COMSOL simulation to fail if the displacement along a given axis changes with a slope less than or equal to -1 along that same axis. If the slope is -1 then two adjacent points collapse to the same point. If the slope is less than -1 then the spatial ordering of the two adjacent points is inverted. This places an upper bound on the amplitudes that can be used for a given λ, or conversely it places a lower bound on λ for a given amplitude, as the peak slope is roughly proportional to the ratio of amplitude to λ.

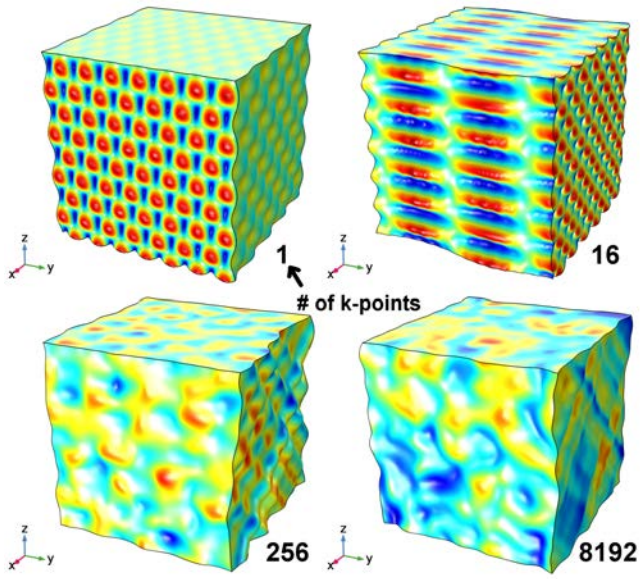

Fig. 2. 250-nm cube structures with surface roughness functions of increasing numbers of $\boldsymbol{k}$-points, contoured with x-component of displacement. Too few points result in evident periodicities, while too many slows execution time. In this paper, 8192 points were used (bottom-right).

In this paper, the function was evaluated once for the mesh to generate a CSV file, then the CSV file was loaded as an "interpolation function" to evaluate the distortion using "material" coordinates, which allow for the deformation of the structure. The Fourier function is normalized by first summing the squares of the initally determined amplitudes and dividing by 2, accounting for the mean of sine^2. All amplitudes are then divided by the square root of this sum.

Fig. 2 shows simple cube structures perturbed with random surface roughness patterns of various numbers of $\boldsymbol{k}$-points (1, 16, 256, and 8192); the surface color/shade indicates the x-component of the displacement. (A y-component of displacement also affects the surface boundary.) With too few $\boldsymbol{k}$-points, the roughness pattern is too regular; this is most evident when only one point is used. With more points, the computation time increases. The results presented in the following used 8192 points (bottom-right case in the figure).

The NEM switch studied in this paper consists of a movable central structure (cantilever), actuation electrodes ("gates") on either side of the structure formed in the two lowermost metal layers, and pairs of contacting electrodes on either side of the structure formed in the uppermost metal layer. The topmost portion of the movable structure, formed in the uppermost metal layer serves to bridge the pair of (left and right) conducting electrodes in the front or in the back, depending on which side the cantilever is actuated.

As a simplification, surface roughness is modeled only in the cantilever structure, and not the gate surfaces or the contacting

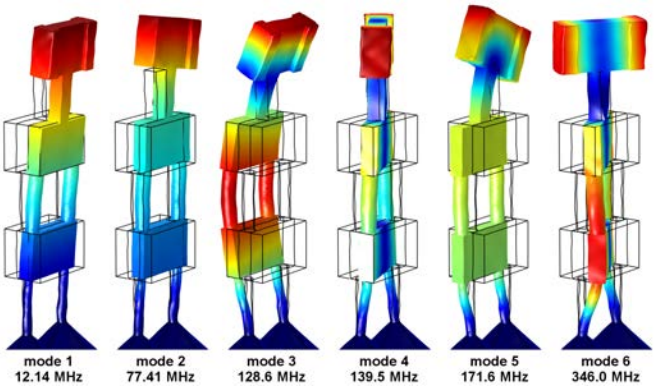

Fig. 3. Exaggerated representation of six lowest linear eigenmodes for the cantilever portion of an NEM switch with 2-nm surface roughness.

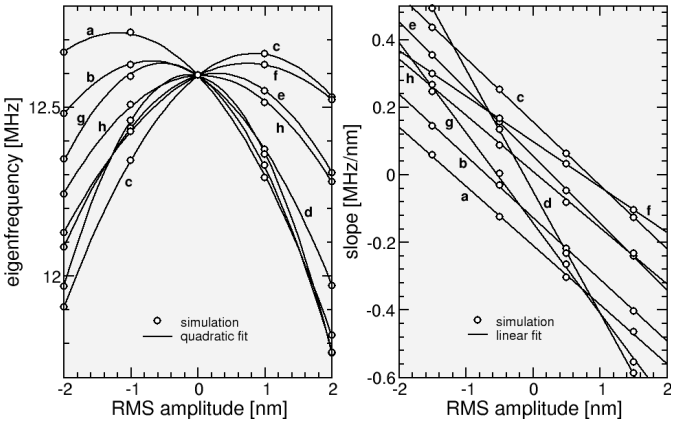

Fig. 4. Left: eigenfrequency versus surface roughness amplitude, for various roughness patterns a–h. The lines represent quadratic fits to the numerically modeled data. Negative amplitude converts valleys into peaks and vice versa. Right: derivative of eigenfrequency versus surface roughness.

electrode surfaces. This is similar to the classic approach of Greenwood and Williamson applied to the modeling of contact resistance [11], and facilitates computation of mechanical contact forces, which can now be specified at each point in terms of the x coordinate and the force in the x-direction, independent of y and z. However, this simplification causes some effects of rough surfaces to be missed: when two rough surfaces are brought into contact by an actuation in the direction of $\hat{x}$, there will be components of the contact force in all the directions ($\hat{x}$, $\hat{y}$, and $\hat{z}$) rather than only in the $\hat{x}$-direction as with the Greenwood and Williamson approach used herein. This affects not only the direction of the contact force but also the influence of friction. Friction causes energy loss, and diminishing its effect by neglecting the tangential contact of dual rough surfaces requires a compensatory increase in an inelasticity term. However, experimentally measured inelasticities will already implicitly include such frictional losses.

With regard to electrostatic actuation force, the effect of neglecting roughness on the actuation electrode surfaces is expected to be small, since the nominal size of the actuation air gap (30 nm) is significantly larger than the correlation length of the surface roughness (10 nm). If this were not the case, adding roughness to the electrode would be relatively straightforward.

IV. Eigenmode Analysis

COMSOL allows for the solution of eigenmodes of a mechanical system. The eigenmode analysis has the advantage of computational efficiency: it uses a linearized system to relatively quickly find the oscillation modes of the structure in the linear small-amplitude limit. Typically, eigenmodes are associated with each bending mode, with a primary eigenmode representing the desired motion, and higher eigenmodes often representing undesired motion which can reduce the controllability of the device by storing kinetic energy. The first six eigenmodes of a cantilever with 2-nm roughness are rendered in Fig. 3. The primary eigenmode is useful for basic switch operation while the fourth eigenmode is useful for accommodating surface roughness on the (pairs of) contacting surfaces. The other eigenmodes are associated with undesirable motions.

The primary-mode eigenfrequency is plotted as a function of surface roughness amplitude in Fig. 4, for various patterns of surface roughness. As can be seen from the left plot, random surface roughness results in eigenfrequency variation, and there is generally a trend of reduction in eigenfrequency with increasing surface roughness amplitude. The numerically modeled data are well fit to quadratic curves, as is evident in the right plot which shows a linear dependence of the slope versus surface roughness amplitude, indicating a second-order dependence similar to (1). The corresponding plots for higher order eigenmodes show similar results.

V. Contact Force Modeling

The upper portion of the cantilever comes into physical contact with a conducting electrode when the x coordinate of one or more points in that portion overlaps the domain of the electrode. An elastic contact model can be applied to the cantilever surface, with a force function defined as follows:

$$F_{\text{contact}} = u_{x-x_0}(x_0 - x)K_{\text{contact}} \tag{3}$$

for the "front" contact located at $x = x_0$ and

$$F_{\text{contact}} = (u_{x+x_0} - 1)(x_0 + x)K_{\text{contact}} \tag{4}$$

for the "back" contact located at $x = -x_0$. u is the Heavyside function: $u_x \equiv 1$ for $x > 0$, 0 for $x < 0$.

Inelasticity is characterized by a loss in kinetic energy upon recoil. This can be modeled by attenuating the force when the cantilever is recoiling relative to the force when the cantilever is approaching contact. For this, a function is needed to describe whether the switch is closing or opening. It is tempting to simply use the sign of the x-component of the velocity of the cantilever; however, this would result in a discontinuity of force with respect to velocity as the local velocity crosses zero, and is thus destabilizing as well as nonphysical. Therefore, instead, we use a sigmoid function to sample the velocity direction. Rather than defining the sigmoid analytically, the COMSOL function-smoothing feature is used, so that the function transitions from 0 to 1 as the velocity goes

from − 10 to 10 cm/s (which are relatively low velocities for an NEM device [12]).

Given this sigmoid function to indicate the sign of the x-component of the velocity, f_{vx}, a lossy contact force function can be defined, for the front contacts

$$F_{\text{contact}} = u_{x-x_0}(x_0 - x)[1 - \eta(1 - f_{vx})]K_{\text{contact}} \quad (5)$$

and for the back contacts

$$F_{\text{contact}} = (u_{x+x_0} - 1)(x_0 + x)(1 - \eta f_{vx})K_{\text{contact}} \quad (6)$$

where in each case, η is the fraction of energy lost in the inelastic recoil. A typical value for η is 0.75, with the recoil speed being half of the incident speed, and kinetic energy proportional to the square of the speed.

The force per unit area on the surface for a given linear compression, K_{contact}, was set to 2 GPa/nm. A physically based estimate can be established by considering colliding spheres [13] to approximate the initial contact of two rough surfaces. Consider two Cu spheres of diameter 5 nm (bulk modulus 123 GPa and Poisson ratio 0.36 [14]). At 1-nm depression, the effective $K_{\text{contact}} = 13.4$ GPa/nm. The smaller value was used here to better resolve the space and time dependence of the contact pressure during collision, subject to the constraint that the peak depression remains a small fraction of other dimensions.

Another source of energy loss is friction, which is a retarding force that opposes sliding motion when surfaces are in contact. For the target surface being a plane normal to the x-axis, then, friction is associated with motion in the yz plane. In a standard friction model, the dynamic friction force against the direction of motion is proportional to the normal force. This model is modified herein with another smoothing function, g_{vxy}, to avoid a discontinuity at zero in-plane velocity

$$F_{\text{friction}} = F_{\text{contact}}\eta_{\text{friction}}g_{vxy} \quad (7)$$

in the direction opposite, the direction of motion projected on the yz plane. η_{friction} is the appropriate coefficient of friction, while the smoothing function $g_{vxy} = 1 - \exp(-v_{xy}/v_0)$, with $v_0 = 10$ cm/s and v_{xy} is the speed in the xy plane. Implementation of this friction model in transient simulations was found to have little effect except to substantially increase execution time.

Contact adhesive forces can affect the force-versus-position relationship, contributing an attractive force when surfaces are proximate, in addition to the repulsive force, and also to inelasticity due to hysteresis. A review of adhesion mechanisms in microscale devices is in [15]. However, these were not included in this model, except as they contribute to energy loss during collision.

VI. Electrostatic Force Modeling

Electrostatic force was modeled via a boundary force implemented using the structural mechanics module

$$F_x = \frac{1}{2}E_x D_x \quad (8)$$

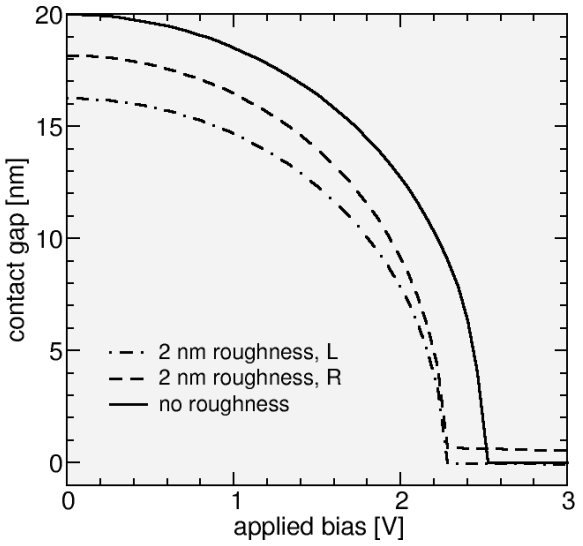

Fig. 5. Effect of surface roughness on contact gap versus gate voltage. With roughness, left and right contact gaps are shown separately. The initial gap is smaller. The smaller gap (L) closes at a lower voltage but the larger gap (R) never fully closes.

where E_x is the x-component the electric field and D_x is the x-component of the displacement field.

For a rough surface or a tilted surface, this is an approximation but the error is the second order; tangential force components will tend to cancel.

The electrostatic potential was solved in "ambient" regions between the cantilever and the constant-potential surfaces used to represent the gate electrodes. To allow the mesh to deform in these ambient regions, the moving mesh module was used, with boundary conditions of zero displacement at the gate electrodes and zero normal displacement on the free surfaces. At the interface with the cantilever, the moving mesh displacement was matched to the geometric displacement at the cantilever surface.

A potential difference between the cantilever and the electrodes at the signal layer would provide an additional electrostatic force. This effect, which is state-dependent, was not included here; instead, equipotential signal lines were assumed. The focus here is on surface roughness effects. However, including this force would be important when modeling the general behavior of the device in operation.

VII. Quasi-Static Analysis

An effect of the rough surface is considered in Fig. 5. Here, the actuation portion of the cantilever structure and the two gates on one side were grounded while the voltage applied to the gates on the opposite side was ramped from 0 to 3 V to actuate the conducting portion of the structure into contact with the pair of conducting electrodes on said opposite side.

For no roughness (i.e., for a perfectly smooth structure), the contact gaps on the left and right sides of the conducting portion of the structure are identical, so only one curve is plotted in Fig. 5 for this case. When the contact gap reaches zero on both sides, an electrical connection is formed between the conducting electrodes. This is how the switch is designed to operate.

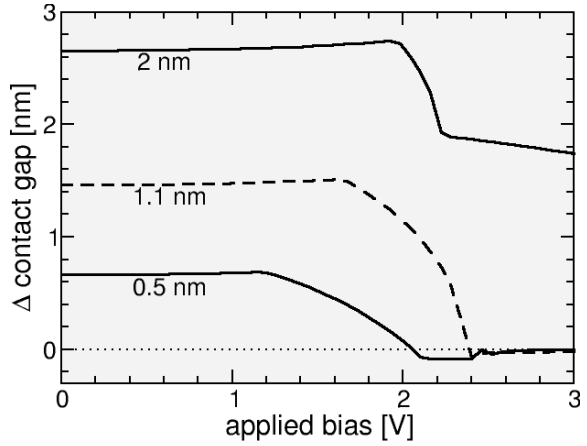

Fig. 6. Difference between left and right contact gaps versus applied gate voltage, for different surface roughness amplitudes.

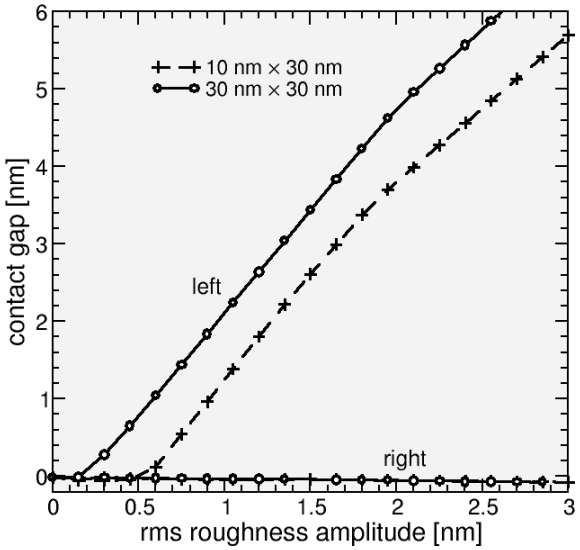

Fig. 7. Gap versus roughness amplitude for the same roughness pattern for two insulator geometries at 3-V bias, a baseline, and an exceptionally thin version for increased torsional compliance. The latter is able to simultaneously close both contacts to 0.5-nm surface roughness amplitude, while the baseline case can tolerate only approximately 0.15 nm of surface roughness.

For the case of 2-nm surface roughness, there are multiple nonideal effects.

1) The initial (0 V) contact gaps are smaller, because they are determined by the most prominent points, and surface roughness tends to result in protrusions extending beyond the nominal surface.
2) The applied voltage at which contact is made is lowered.
3) Torsional stiffness of the structure can prevent contact from being made on both left-hand and right-hand sides, so that an electrical connection between the conducting electrodes is not formed. (In Fig. 5 the contact gap never reaches 0 for the right-hand side.)

This result highlights the need for the structure to have either adequately small surface roughness or sufficient compliance to operate properly.

Fig. 6 plots the difference between the left and right contact gaps as a function of the applied actuation voltage, for various values of surface roughness amplitude. An electrical connection is made between the conducting electrodes only when the gap difference is essentially zero.

To reduce the sensitivity of the NEM switch functionality to surface roughness, the structure must be able to rotate more readily to accommodate bilateral asymmetry. One way to achieve this is to make the dielectric post narrower. Fig. 7 shows how the left and right contact gaps depend on surface roughness when the applied gate voltage is fixed at 3 V, comparing a "baseline" 30-nm-wide postdesign with a narrower 10-nm-wide postdesign. In this example, the right contact gap is closed for 3-V applied voltage, but the left contact gap is closed (i.e., the switch operates properly) only if the surface roughness amplitude is less than 0.15 nm, for the baseline design. With a more compliant post, the tolerable level of surface roughness is increased to approximately 0.5 nm.

To study the relative contributions from the two gate levels, the bias between a smooth cantilever and a gate on one side was ramped, biasing either the top or bottom gate but not both. The force ratio was estimated as the inverse ratio of the voltage-squared needed to reach a given displacement. This ratio was 3.1 in the zero-displacement limit, increasing to 4.8 at 15-nm deflection. Thus, the top gate is substantially more effective at bending the cantilever than the bottom gate, contributing more than 75% of the deflection, with the fraction increasing as the deflection disproportionately decreases the electrostatic gap to the top gate. Removing the bottom gate would require only a 10% increase in the voltage applied to the top gate to close the contact gap.

VIII. Transient Analysis

For transient analysis, the device is initially in the equilibrium state, with 0 V applied to the actuation portion of the cantilever and to both the front and back sets of gates, such that the cantilever is not deformed. Then, to operate the device as a single-pole/double-throw switch, one set of gates is biased at 0 V while the other set is biased at V_{DD}. A time-dependent voltage signal (ranging from 0 V to V_{DD}) applied to the actuation portion of the cantilever causes the conducting portion of the cantilever to move into (or out of) contact with the sets of conducting electrodes on the front and back side.

To evaluate the transient response, the time-dependent positions of four discrete points on the conducting portion of the cantilever structure are plotted. The points of principal interest are those with the greatest x coordinates on the left-hand and right-hand sides of the "front" surface, and those with the least x coordinates on the left-hand and right-hand sides of the "back" surface.

Fig. 8 shows the transient response of a typical cantilever with 1-nm surface roughness in response to a rapidly changing voltage signal applied to the actuation portion of the cantilever structure. Although quasi-static simulation of this structure showed that both the left and right contact gaps do not close, transient simulation shows that both gaps close (albeit only temporarily) due to inertia.

Fig. 9 shows the same device with an applied voltage signal that changes less frequently. Contact bounce is seen, with

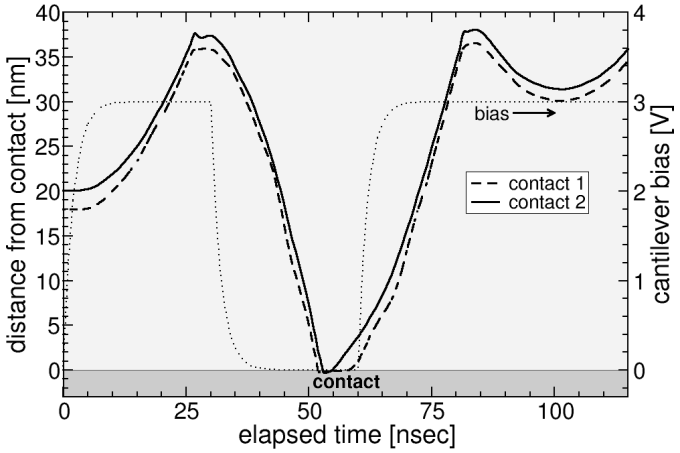

Fig. 8. Transient response for a structure with 1-nm surface roughness amplitude. The voltage applied to the actuation portion of the cantilever is shown as a dotted line (right *y*-axis).

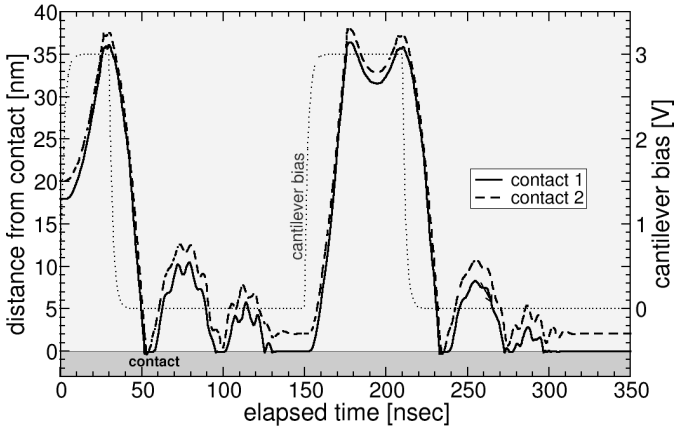

Fig. 9. Transient response for less frequent switching, including friction modeling.

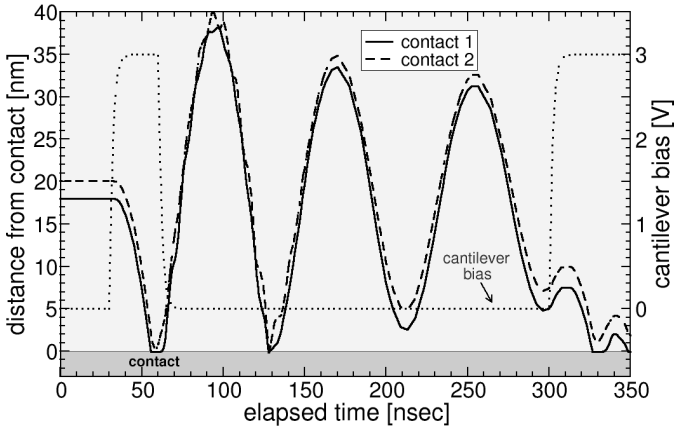

Fig. 10. Transient response for device operation as a tristate switch.

the structure settling into a state in which only one (left or right) side is in contact. This is because after inelastic bouncing kinetic energy is lost, leaving insufficient momentum to overcome the torsional stiffness upon subsequent impact.

The structure studied in this paper could be operated as a tristate switch, in which the OFF-state corresponds to the equilibrium (noncontacting) state. The transient response for this operation mode is shown in Fig. 10, for the case where two short voltage pulses are applied to turn ON the switch and there is a relatively long period of time in-between these pulses. Oscillatory behavior occurs when the switch is turned OFF, which can result in undesirable variation in turn-ON delay and failed switch operation (if both the left and right contact gaps do not close). To avoid these issues, the switching frequency must be reduced to allow the oscillations to attenuate sufficiently between turn-ON events.

IX. Conclusion

Effects of surface roughness on the operation of a nanometer-scale electromechanical (NEM) switch implemented using CMOS BEOL layers were examined in this paper. The roughness itself was generated using a 3-D Fourier function with randomized coefficients implementing a Gaussian roughness model, with the $\boldsymbol{k}$-dependence of the amplitude of the normally distributed coefficients established using a low-pass filter to match the desired autocorrelation length.

The effects of surface roughness include the following.

1) Eigenfrequencies for oscillation modes are reduced, on average.
2) Assymetry in contact gap sizes can result in failed switch operation, if the surface roughness amplitude is too large.

The latter effect is most evident for the quasi-static operation. Under rapid switching conditions, inertia can help to close the contact gaps to ensure proper switch operation, but also can result in contact bounce.

These results make it clear that in the presence of surface roughness, the NEM switch design investigated herein must have sufficient torsional compliance to function properly. More generally, surface roughness must be included to accurately model the statistical mean characteristic of an NEM switch.

References

[1] H. Kam, V. Pott, R. Nathanael, J. Jeon, E. Alon, and T.-J. K. Liu, "Design and reliability of a micro-relay technology for zero-standby-power digital logic applications," in *IEDM Tech. Dig.*, Dec. 2009, pp. 809–812.

[2] F. Chen, H. Kam, D. Markovic, T.-J. K. Liu, V. Stojanovic, and E. Alon, "Integrated circuit design with NEM relays," in *Proc. IEEE/ACM Int. Conf. Comput.-Aided Design*, Nov. 2008, pp. 750–757.

[3] S. Natarajan *et al.*, "A 14 nm logic technology featuring 2^{nd}-generation FinFET, air-gapped interconnects, self-aligned double patterning and a 0.0588 μm^2 SRAM cell size," in *Proc. IEEE Int. Electron Devices Meeting*, Dec. 2014, pp. 3.7.1–3.7.3.

[4] N. Xu *et al.*, "Hybrid CMOS/BEOL-NEMS technology for ultra-low-power ic applications," in *IEDM Tech. Dig.*, Dec. 2014, pp. 677–680.

[5] K. Kato, V. Stojanovic, and T.-J. K. Liu, "Non-volatile nano-electro-mechanical memory for energy-efficient data searching," *IEEE Electron Device Lett.*, vol. 37, no. 1, pp. 31–34, Jan. 2016.

[6] *Comsol Multiphysics V. 5.2a*, Comsol AB, Stockholm, Sweden, 2016. [Online]. Available: http://www.comsol.com

[7] B. F. Toler, R. A. Coutu, Jr., and J. W. McBride, "A review of micro-contact physics for microelectromechanical systems (MEMS) metal contact switches," *J. Micromech. Microeng.*, vol. 23, no. 10, p. 103001, Sep. 2013.

[8] K. El Sayed, A. Wettstein, S. D. Simeonov, E. Lyumkis, and B. Polsky, "Investigation of the statistical variability of static noise margins of SRAM cells using the statistical impedance field method," *IEEE Trans. Electron Devices*, vol. 59, no. 6, pp. 1738–1744, Jun. 2012.

[9] M. S. Longuet-Higgins, "Statistical properties of an isotropic random surface," *Phil. Trans. Roy. Soc. London A: Math., Physi. Eng. Sci.*, vol. 250, no. 975, pp. 157–174, Oct. 1957. [Online]. Available: http://rsta.royalsocietypublishing.org/content/250/975/157
[10] R. J. Adler and D. Firman, "A non-Gaussian model for random surfaces," *Phil. Trans. Roy. Soc. London A: Math., Physi. Eng. Sci.*, vol. 303, no. 1479, pp. 433–462, Dec. 1981. [Online]. Available: http://rsta.royalsocietypublishing.org/content/303/1479/433
[11] J. Greenwood, "A unified theory of surface roughness," *Proc. Roy. Soc. A*, vol. 393, pp. 133–157, May 1984.
[12] C. Qian, A. Peschot, D. J. Connelly, and T.-J. K. Liu, "Energy-delay performance optimization of NEM logic relay," in *IEDM Tech. Dig.*, Dec. 2015, pp. 18.1.1–18.1.4.
[13] M. J. Puttock and E. G. Thwaite, "Elastic compression of spheres and cylinders at point and line contact," Nat. Standards Lab. Commonwealth Sci. Ind. Res. Org., Canberra, Australia, Tech. Rep. 25, 1969.
[14] *The Engineering ToolBox: Metals and Alloys—Bulk Modulus*, accessed on Mar. 2017. [Online]. Available: http://www.engineeringtoolbox.com/bulk-modulus-metals-d_1351.html
[15] R. Maboudian and R. T. Howe, "Critical review: Adhesion in surface micromechanical structures," *J. Vac. Sci. Technol. B*, vol. 15, no. 1, pp. 1–20, Nov. 1997.

Daniel Connelly received the Ph.D. degree from Stanford University, Stanford, CA, USA.

He was with Acorn Technologies, Palo Alto, CA, USA where he worked on advanced CMOS technology development, with Synopsys, Mountain View, CA, USA, where he worked on device simulation and modeling, and with Poet Technologies, an Jose, CA, USA. He is currently a Visiting Scholar with the University of California at Berkeley, Berkeley, CA, USA.

Tsu-Jae King Liu (SM'00–F'07) received the B.S., M.S., and Ph.D. degrees in electrical engineering from Stanford University, Stanford, CA, USA, in 1984, 1986, and 1994, respectively.

Since 1996, she has been a Faculty Member with the Department of Electrical Engineering and Computer Sciences, University of California, Berkeley, CA, USA, where she is currently the TSMC Distinguished Professor in microelectronics of electrical engineering and computer sciences.